Ultrasonics 99 (2019) 105974

Contents lists available at ScienceDirect

Ultrasonics

journal homepage: www.elsevier.com/locate/ultras

Simultaneous measurements of ultrasound attenuation, phase velocity, thickness, and density spectra of polymeric sheets

Kazuto Tsuji, Tomohisa Norisuye*, Hideyuki Nakanishi, Qui Tran-Cong-Miyata

Department of Macromolecular Science and Engineering, Graduate School of Science & Technology, Kyoto Institute of Technology, Matsugasaki, Sakyo-ku, Kyoto 606-8585, Japan

ARTICLE INFO

Keywords:
Attenuation coefficient
Phase velocity
Ultrasonic spectroscopy
Ultrasound scattering

ABSTRACT

The size distribution and mechanical properties of microparticle dispersed in liquid can be characterized by ultrasonic spectroscopy with the aid of acoustic scattering theories. In order to carry out the accurate analysis of the particles, the basic properties, such as the density, viscosity, longitudinal and shear velocities and intrinsic attenuation coefficient of the particle must be known prior to the analysis. Particularly, for soft elastomers or rubbers which exhibit complex mechanical properties with comparable real and imaginary parts, such fundamental information should be provided prior to the particle analysis to minimize the uncertainty of estimation associated with the number of adjustable parameters. In this study, we examined the acoustical properties of poly(methyl methacrylate)(PMMA) and cross-linked poly(dimethyl siloxane) sheets having different cross-linker concentrations by Multiple-Echo Reflection Ultrasonic Spectroscopy which simultaneously enabled us to acquire 4 fundamental properties, the ultrasound attenuation coefficient, phase velocity, density, and thickness (MERUS4 for solid plate). In addition, it was confirmed that the acoustic spectra of PMMA particles dispersed in water were reproduced well with the physical properties determined by MERUS4 using the PMMA plates.

1. Introduction

Ultrasonic spectroscopy (US) is a powerful tool to evaluate the mechanical and/or viscoelastic properties of materials in the ultrasonic frequency regime. For example, US has been utilized to study the local dynamics and properties of bulk polymers, polymer solutions and networks, and also to monitor the reaction processes such as gelation of acrylamide hydrogels [1], polyurethane [2], epoxy [3], and whey proteins [4]. When elastic microparticles were dispersed in a liquid, or embedded in a solid matrix, the size distribution as well as the elastic properties of individual particles were evaluated by acoustic scattering analysis without dilution or drying of the sample [5–12]. In addition, the shell thickness and/or the elasticity of microcapsule were also examined by the ultrasonic analysis [10,13].

For particles whose elastic properties are well-known, the size distribution may be easily determined by the acoustic spectra. On the other hand, when the physical properties are unknown, there is a serious uncertainty to uniquely determine the size distribution of particles. Particularly, when soft elastomer or rubbers, which contain comparable real and imaginary parts of elastic constants are studied, the fundamental physical properties such as the attenuation coefficient, phase velocity, and density, should be accurately determined prior to the particle scattering analysis. It is noted that the acoustic properties must be evaluated as a function of frequency to subsequently carry out the scattering function analysis of particle suspensions. For these reasons, an analysis method for determination of the longitudinal attenuation coefficient, phase velocity, and density of plastic sheets was explored in this study. Note that it would be better to simultaneously evaluate the thickness of the elastomer sheet by ultrasound since the thickness measured by a conventional thickness gauge could be seriously underestimated due to deformation during the measurement.

The purpose of this study is to develop a technique which allows us to acquire the acoustic properties as well as the thickness of plastic and elastomer sheets. This technique also provides the information on the cross-link density dependence of the acoustical properties. The obtained information could be utilized in the further analysis of particle suspension, which requires more elaborate investigation, e.g., soft elastomer or rubber particles having comparable real (elastic) and imaginary (viscous) contributions. In this study, the cross-linked elastomer sheet is of particular interest. However, once the cross-linked network is formed by a chemical reaction, it is difficult to prepare spherical microparticles from the elastomer sheet or thermoset plastic sheet with equivalent ultrasonic properties. On the contrary, poly(methyl methacrylate) (PMMA) particles can be easily recasted from a piece of PMMA

* Corresponding author.
E-mail address: nori@kit.jp (T. Norisuye).

https://doi.org/10.1016/j.ultras.2019.105974
Received 19 April 2019; Received in revised form 22 July 2019; Accepted 1 August 2019
Available online 09 August 2019
0041-624X/

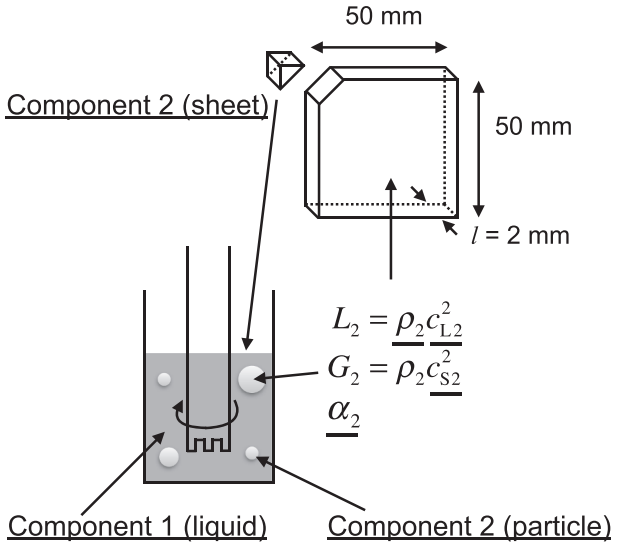

Fig. 1. Preparation method of the particles having acoustical properties equivalent to the solid sheet.

sheet. The strategy of this work is schematically illustrated in Fig. 1. Ultrasound propagation in the suspension consisting of polymeric particles (component 2), the surrounding liquid (component 1), and the polymeric sheet samples (approximately 50 mm × 50 mm × 2 mm) having the equivalent acoustical properties for the component 2 are studied here. This allows us to carry out the scattering function analysis of the PMMA particles in suspensions using all the given parameters, such as the density ρ_2, longitudinal velocity c_{L2}, shear velocity c_{S2}, the attenuation coefficient α_2, longitudinal modulus L_2 and the shear modulus G_2 independently determined by ultrasonic spectroscopy and the mode conversion technique of the PMMA sheets.

As for a liquid sample in a cell, the technique enabling the simultaneous measurement of the 3 acoustical properties, attenuation coefficient α, phase velocity c and density ρ utilizing Multiple-Echo-Reflection-Ultrasonic Spectroscopy (hereafter abbreviated as MERUS3 for liquid) has already been available [14,15]. On the contrary, the technique developed in this study deals with a solid plate. In addition to α, c, and ρ, the sample thickness l can be evaluated simultaneously. Since the technique provides 4 multi-parameters simultaneously by utilizing multiple echo of reflected ultrasonic pulses, hereafter the method is abbreviated as MERUS4 for solid plate.

2. Experimental procedure

2.1. Materials

Tetraethylorthosilicate (TEOS), stannous octanoate (STO) were purchased from Tokyo Chemical Industry Co., JAPAN. α, ω-dihydroxypoly(dimethylsiloxane) (PDMS, X-21-5841) was purchased from Shin-Etsu Chemical Co., JAPAN. All the chemical reagents were used without further purification. Acrylite™, an acrylic resin mainly composed of poly(methyl methacrylate) (PMMA), was purchased from Mitsubishi Chemical Co. Japan. Unplasticized polyvinyl chloride (uPVC) sheets was purchased from Takiron C. I., Japan. High-density polyethylene (HDPE), polypropylene (PP), polycarbonate (PC) sheets were purchased from Plaport Co., Japan. Polyphenylenesulfide, PPS was purchased from Toray Plastics Precision Co., Ltd., Japan.

2.2. Preparation of PDMS sheets

Cross-linked PDMS sheets were prepared by hydrolysis and condensation reactions of PDMS and TEOS in the presence of STO as a catalyst. Prescribed amounts of TEOS (w_{TEOS}) and STO (w_{STO}) represented in Table 1 were dissolved in PDMS (w_{PDMS}). The ratio of the TEOS weight to the total weight defined by

$$C_x = \frac{w_{TEOS}}{w_{TEOS} + w_{PDMS}} \times 100 \quad (wt\%), \tag{1}$$

was used as a measure of the cross-linking density and was abbreviated as Cx1 to Cx7. After complete dissolution, the solution was poured into a polystyrene dish, and placed on a horizontal table (e.g., 1 h for Cx7) to complete the reaction.

Table 1
The composition of materials for preparation of the PDMS sheets.

	Cx1	Cx2	Cx3	Cx4	Cx5	Cx6	Cx7
w_{PDMS} (g)	7.9999	8.0034	8.0072	8.0019	8.0011	8.0007	8.0032
w_{TEOS} (g)	0.0800	0.1645	0.2433	0.3374	0.4224	0.5096	0.6075
w_{STO} (g)	0.2456	0.2526	0.2559	0.2574	0.2650	0.2623	0.2678

2.3. Preparation of PMMA particles from a PMMA sheet

After the ultrasonic measurements of the PMMA sheets, 8 g of PMMA was dissolved in 30 g of acetone, and aged for several days to obtain the homogeneous stock solution. Then, 1.2 g of the solution was mixed with 6 g of toluene to prepare the PMMA/acetone/toluene solution with the ratio 1:4:24. Subsequently, 4 g of the solution was mixed with 250 g of sodium dodecyl sulfate (SDS) aqueous solution by a magnetic stirrer at 70 °C. The solution was stirred at 1000 rpm at beginning, followed by slow mixing at 200 rpm for 5 h. The particles were imaged using a phase-contrast optical microscope (Nikon, model OPTIPHOT-2) equipped with a CCD camera. The PMMA particles having a broad size distribution (from submicron to 100 μm) were fractionated by using a nylon mesh filter with the pore size 10 or 20 μm. The resultant average particle diameter $< d >$ and the coefficient of variation (the standard deviation normalized by the average diameter) CV were respectively 15.0 μm and CV = 0.18. Thus obtained particles are washed with a large amount of water, and annealed at 85 °C to obtain the dried powder.

2.4. Ultrasonic spectroscopy

An ultrasound pulse was generated using a broadband pulser/receiver (JSR DPR500) with a remote pulser RP-H4 or RP-L2. Water-immersion longitudinal plane wave transducers having different nominal frequencies, such as B5K6I (element diameter of transducer d_{TD} = 6 mm, 5 MHz), B10K2I (2 mm, 10 MHz), B20K1I (1 mm, 20 MHz) and B30K1I (1 mm, 30 MHz) manufactured by KGK (Japan), were employed to examine the frequency dependences of the acoustical properties of the materials. The transmitted pulse was received by another transducer, followed by the amplification using the receiver.

The distance of the transducer-to-plate, x and the transducer to transducer, D were respectively x = 49, 25, 15, and 25 mm and D = 100, 43, 32, and 43 mm for B5K6I, B10K2I, B20K1I and B30K1I. These paths were important to avoid the contribution from the edge wave [14,16]. The interference of the direct beam and edge waves occurs when the condition $x - \sqrt{x^2 - \frac{d_{TD}^2}{4}} = \frac{\lambda}{2}n$ is satisfied where λ is the wavelength of ultrasound, n is an integer. Then, the critical distance may be given by $x = \frac{d_{TD}^2}{4\lambda} + \frac{\lambda}{4} \cong \frac{d_{TD}^2}{4\lambda}$. This is equivalent to the equation of the near field distance of continuous waves although the physical origin is completely different. Since the theoretical critical distances are respectively, x = 30, 6.7, 3.3 and 5 mm for B5K6I, B10K2I, B20K2I and B30K1I, the experimental distances were kept sufficiently longer than the critical distance. For the measurement of liquid sample in a cell, the receiving transducer was placed 10 mm further compared to the above condition.

The solid plate (or sample cell for liquid sample) and transducer

were carefully aligned by a homemade stainless stage equipped with microstages. Particularly, the sample tilt was carefully checked to maximize the echo signal (± 0.007° in our case). The transmitted and echo signals were recorded by a 12-bit high-speed digitizer, GaGe CS121G2, at a sampling rate of 1 Giga samples/s. The trigger timing was controlled by using a square pulse generated by an arbitrary wave generator (Keysight Technologies, 33521B). A digital delay (Stanford, DG645) was employed to control the acquisition timing of the input and output signals by taking account of the traveling time of sound in water. The digital equipment was synchronized with a 10 MHz reference clock to avoid phase jittering. The pulse repetition time was set at 0.5 ms and the pulse was averaged over 5000 times to achieve good precision. The sample was set in a homemade thermostat bath regulated at 25 ± 0.005 °C. The temperature stability was confirmed by measuring the stability of the phase velocity obtained over 6 digits for deuterated water using multi-echo reflection ultrasonic spectroscopy (MERUS3 for liquid) [14,15] described later.

3. Ultrasonic spectroscopy methods

3.1. Multiple-echo-reflection ultrasonic spectroscopy for solid plates (MERUS4 for solid plate)

Since we have four unknown variables, i.e., the intensity (power) attenuation coefficient α, phase velocity c, density ρ, and thickness l of a solid sheet for the longitudinal mode, the corresponding numbers of equation are required to solve them simultaneously. The first equation is obtained from the transmitted signal through the solid plate. As schematically illustrated in Fig. 2, the Fourier transformation of the transmitted longitudinal pulse through the sample, $T^*$and the reference pulse, T_0^*, and the multiply reflected transmitted signal, T'^*, were obtained as a function of the frequency, f.

The ratio of the frequency spectra, $\frac{T'^*(f)}{T^*(f)}$, includes the information on the energy reduction and the phase difference associated with sound propagation through the sample with the thickness l. Then, $\frac{T'^*(f)}{T^*(f)}$ is expressed by,

$$\frac{T'^*(f)}{T^*(f)} = \frac{|T'^*|}{|T^*|}\exp[\mathrm{i}(\theta' - \theta)] = \frac{e^{3\mathrm{i}k_1 l} e^{\mathrm{i}k_0(D-l)} t_{01}^* t_{10}^* (r_{10}^*)^2}{e^{\mathrm{i}k_1 l} e^{\mathrm{i}k_0(D-l)} t_{01}^* t_{10}^*} = (r_{10}^*)^2 e^{2\mathrm{i}k_1 l}, \quad (2)$$

where $\mathrm{i} = \sqrt{-1}$,

$$k_1 = \frac{2\pi f}{c} + \mathrm{i}\frac{\alpha}{2}, \quad (3)$$

and

$$k_0 = \frac{2\pi f}{c_0} + \mathrm{i}\frac{\alpha_0}{2}, \quad (4)$$

are the wavenumber of the solid plate sample and the water, t_{01}^* and r_{01}^* are the transmission and reflection coefficient between water 0 and sample 1, and D is the distance between transducers in the transmission setup, $\frac{|T'^*|}{|T^*|}$ and $\theta' - \theta$ are respectively the amplitude ratio and the phase difference of $\frac{T'^*(f)}{T^*(f)}$. Note that the factor 2 appeared in the denominator of the imaginary part of the wavenumbers k_1 and k_0 is originated from the definition of the intensity (power) attenuation representing the energy dissipation of ultrasound. The values of c_0 and α_0/f^2 at 25 °C are 1496.7 (m/s) and 4.38×10^{-14} (s^2 Np/m) repectively [17,18]. The effect of incident pulse and all other effects before arriving at the sample are cancelled out in both nominator and denominator of the second line of Eq.(2).

In order to eliminate $(r_{10}^*)^2$ from Eq. (2), another equation is required. With the pulse echo setup, the ratio,

$$\frac{R_B^*(f)}{R_A^*(f)} = \frac{t_{01}^* r_{10}^* t_{10}^* e^{2\mathrm{i}k_1 l}}{r_{01}^*} = -t_{01}^* t_{10}^* e^{2\mathrm{i}k_1 l} = [(r_{10}^*)^2 - 1]e^{2\mathrm{i}k_1 l}, \quad (5)$$

can be obtained where R_A^* and R_B^* are Fourier transformation of the reflected pulse waveform before and after passing through the sheet, respectively. This also contains contributions from the reflection loss and propagation in the solid plate. By eliminating $e^{2\mathrm{i}kl}$ from (2) and (5), one obtains,

$$(r_{10}^*)^2 = 1 - t_{01}^* t_{10}^* = \frac{(T'^*/T^*)}{(T'^*/T^*) - (R_B^*/R_A^*)} \quad (6)$$

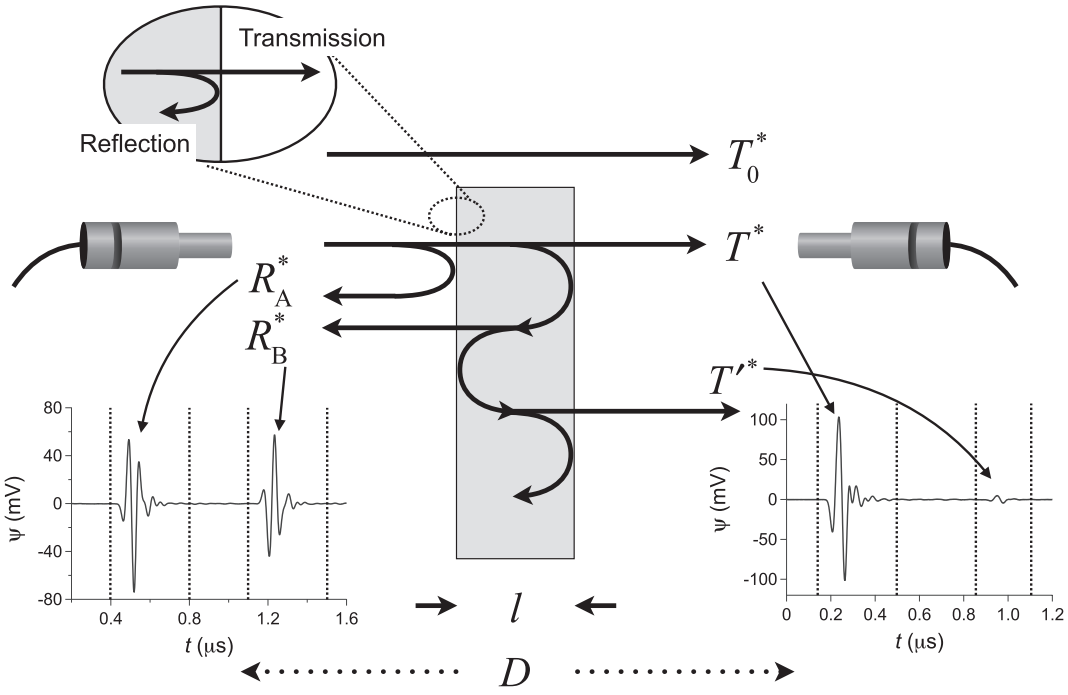

Fig. 2. Schematic illustration of transmission and reflection signals utilized in the MERUS4 analysis.

Finally, to evaluate α and c, the ratio of the sample signal $T^*$to the reference T_0^*,

$$\begin{aligned}\frac{T^*(f)}{T_0^*(f)} &= \frac{|T^*|}{|T_0^*|}e^{i(\theta-\theta_0)} \\ &= \frac{e^{ik_1 l}e^{ik_0(D-l)}t_{01}^*t_{10}^*}{e^{ik_0 D}}, \\ &= t_{01}^*t_{10}^*e^{i(k_1-k_0)l} \\ &= [1-(r_{10}^*)^2]e^{i(k_1-k_0)l}\end{aligned} \tag{7}$$

is analyzed. Since the phase part of Eq. (7) is written as,

$$\theta-\theta_0 = 2\pi f l\left[\frac{1}{c}-\frac{1}{c_0}\right] + \arg[1-(r_{10}^*)^2] + 2m\pi, \tag{8}$$

the phase velocity can be given by,

$$c = \frac{2\pi f l}{(\theta-\theta_0) - \arg[1-(r_{10}^*)^2] - 2m\pi + \frac{2\pi f l}{c_0}} \tag{9}$$

Evaluation of the appropriate number of m, is described elsewhere [14]. On the other hand, from Eq. (2), one obtains,

$$l(f) = \frac{c(f)}{2\pi f}(\theta' - \theta - \arg[(r_{10}^*)^2] - 2m\pi) \tag{10}$$

By substituting Eq. (10) into Eq. (9), one obtains,

$$c(f) = c_0\left[1 - \frac{2\{\theta-\theta_0-\arg[1-(r_{10}^*)^2]-2m\pi\}}{\theta'-\theta-\arg[(r_{10}^*)^2]-2m\pi}\right] \tag{11}$$

Eqs. (11) and (6) allow us to evaluate the frequency spectra of c from all the experimentally accessible quantities. Thus obtained c is substituted again into Eq. (10) followed by averaging over the frequency to determine the thickness l. Note that although the thickness is a physical parameter which is independent of the frequency, it might be better to leave the thickness data as a function of frequency (without averaging) to compensate possible error on the frequency spectra associated with the unfavorable interference of the signal. Further, from Eq. (7), the attenuation coefficient is expressed as,

$$\alpha(f) = \alpha_0(f) - \frac{2}{l}\left[\ln\frac{|T^*|}{|T_0^*|} - \ln|1-(r_{01}^*)^2|\right] \tag{12}$$

Finally, since the reflection coefficient between the sample 1 and reference 0 is related to the difference between the acoustic impedance, ρ is given by,

$$\rho(f) = \rho_0\frac{k_1}{k_0}\frac{1+r_{01}^*}{1-r_{01}^*} \tag{13}$$

where $\rho_0 = 997$ (kg/m^3) is the density of the reference (water) at 25 °C. The technique described here is similar to the method proposed in the literatures [19,20], but the MERUS4 technique (for solid plate) allows us to simultaneously evaluate the attenuation coefficient, phase velocity, density and thickness of a solid plate as a function of frequency.

3.2. Multiple-echo-reflection ultrasonic spectroscopy for liquid samples in cell (MERUS3 for liquid)

The longitudinal attenuation coefficient α, longitudinal phase velocity c and the density ρ of liquid samples in a cell can be simultaneously evaluated by the following method. Since the detail of the method has already been described previously [14,15], only the outline is briefly addressed here. When an ultrasound pulse is impinged on the rectangular disposal vessel containing a liquid sample, four reflected echoes A^*, B^*, C^* and D^* are observed as schematically illustrated in Fig. 3.

α and c are evaluated using the Fourier transformation of the second echo waveform B_2^* and that of the third echo C_2^* for the sample. The ratio of these pulses is expressed as,

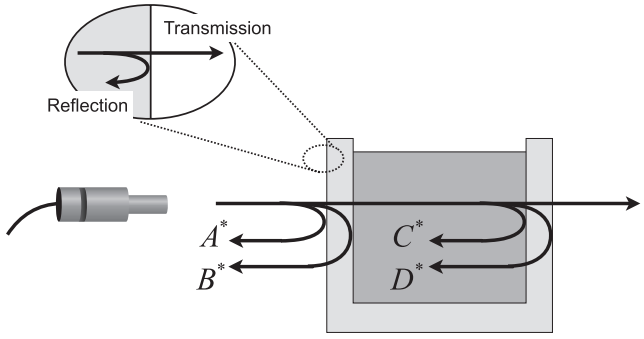

Fig. 3. Schematic illustration of reflection echoes utilized in the MERUS3 analysis.

$$\frac{C_2^*}{B_2^*} = \frac{|C_2^*|}{|B_2^*|}\exp(i\Delta\theta_2) = -t_{12}^*t_{21}^*\exp[2ik_2L], \tag{14}$$

where L is the sample thickness, subscripts 1 and 2 respectively denote the wall and the sample, and k_2 is the wavenumber of the sample given by,

$$k_2 = \frac{2\pi f}{c} + i\frac{\alpha}{2} \tag{15}$$

Above Eq. (14) contains information of sample but the effect of transmission coefficient, $t_{12}^*t_{21}^*$, needs to be corrected, and L must be precisely determined prior to the evaluation of α.

Then, similar equation for the reference,

$$\frac{C_0^*}{B_0^*} = \frac{|C_0^*|}{|B_0^*|}\exp(i\Delta\theta_0) = -t_{10}^*t_{01}^*\exp[2ik_0L] \tag{16}$$

is considered where k_0 is the wavenumber of the reference (water) 0 and $\frac{|C_0^*|}{|B_0^*|}$ and $\Delta\theta_0$ are respectively the amplitude ratio and the phase difference of Eq. (16). From Eq. (16),

$$L = \frac{c_0}{4\pi f}[\Delta\theta_0 - \arg[(r_{10}^*)^2 - 1] - 2m\pi] \tag{17}$$

can be derived. Although determination of the precise thickness requires correction of the reflection coefficient, for pure water, $\arg[(r_{10}^*)^2 - 1]$ could be approximated as π, and then L may be obtained by $L \cong \frac{c_0}{4\pi f}[\Delta\theta_0 - 2(m+1)\pi]$.

In order to correct the reflected energy, the ratio of the second echoes for the sample B_2^* and the reference B_0^*,

$$\frac{B_2^*/A_2^*}{B_0^*/A_0^*} = \frac{t_{01}^*r_{12}^*t_{10}^*e^{2ik_1d}/r_{01}^*}{t_{01}^*r_{10}^*t_{10}^*e^{2ik_1d}/r_{01}^*} = \frac{r_{12}^*}{r_{10}^*} \tag{18}$$

is taken. This gives the reflection coefficient, r_{12}^*, between the sample 2 and the cell wall 1 as,

$$r_{12}^* = r_{10}^*\frac{A_0^*B_2^*}{A_2^*B_0^*} \tag{19}$$

Note that although it is obvious that A_0^* and A_2^* are equivalent, it is better to leave the variables A_0^* and A_2^* in Eq. (19) to compensate the possible error associated with the stability of the signals. For polystyrene disposal cell, $c_1 = 2330$ (m/s), $\rho_1 = 1050$ (kg/m^3), $\alpha_1 = 290$ (Np/m) at 20 MHz were employed to calculate the reflection coefficient between the plastic cell wall and the reference given by,

$$r_{01}^* = \frac{\rho_1c_1^* - \rho_0c_0^*}{\rho_1c_1^* + \rho_0c_0^*} \tag{20}$$

From Eqs. (14) and (17), we obtain,

$$\begin{aligned}c(f) &= \frac{4\pi f L}{\Delta\theta_2 - \arg[(r_{10}^*)^2-1] - 2m\pi} \\ &= c_0\frac{\Delta\theta_0 - \arg[(r_{10}^*)^2-1] - 2m\pi}{\Delta\theta_2 - \arg[(r_{12}^*)^2-1] - 2m\pi}\end{aligned} \tag{21}$$

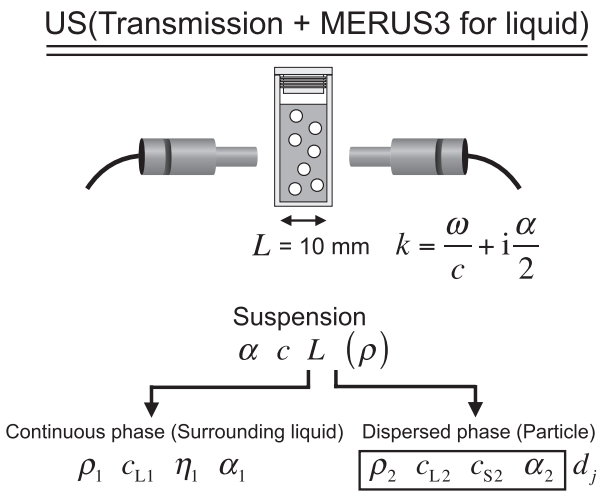

Fig. 4. Schematic illustration of transmission ultrasonic spectroscopy.

Eq. (21) with Eqs. (19) and (20) allows us to obtain precise frequency spectra of c. Similarly, α is obtained by

$$\alpha(f) = -\frac{1}{L}\ln\left[\frac{1}{|(r_{12}^*)^2 - 1|}\frac{|C_2^*|}{|B_2^*|}\right] \tag{22}$$

Finally, since

$$r_{12}^* = \frac{\rho c^* - \rho_1 c_1^*}{\rho c^* + \rho_1 c_1^*}, \tag{23}$$

ρ is derived from Eq. (23) with (19) as,

$$\rho(f) = \rho_1 \frac{k_2}{k_1}\frac{1 + r_{12}^*}{1 - r_{12}^*} \tag{24}$$

3.3. Transmission-ultrasonic spectroscopy for particle suspension (US)

The frequency dependence of the intensity attenuation coefficient, α, and the phase velocity of longitudinal ultrasound, c, were acquired by ultrasound transmission spectroscopy [10,12–15,21] as schematically illustrated in Fig. 4. They were analyzed using the following relationsSPS]code="OT" instruction="Others" / > ,

$$\alpha = -\frac{2}{L}\left\{\ln\frac{|T^*|}{|T_0^*|} - \ln\frac{|t_{12}^* t_{21}^*|}{|t_{10}^* t_{01}^*|}\right\} + \alpha_0 \tag{25}$$

$$c = \frac{2\pi f L}{\theta - \theta_0 - \arg\frac{t_{12}^* t_{21}^*}{t_{10}^* t_{01}^*} + \frac{2\pi f L}{c_0} + 2m\pi} \tag{26}$$

Although the transmission loss due to mismatch of the acoustic impedance between the sample and the cell wall is small, the effect is corrected by an iterative method [22].

The theoretical values of α and c for particle suspensions were calculated using the real and imaginary part of the effective wavenumber k_2. The effective wavenumber of the suspension k_2 are correlated by the dispersion relation [23–26]. In this study, the Lloyd-Berry equation [25],

$$\left(\frac{k_2}{k_0}\right)^2 = 1 + \sum_j \left\{\frac{4\pi N_j(d_j)F_j(0)}{k_0^2} - \frac{4\pi^2 N_j^2(d_j)}{k_0^4}\left[\begin{array}{c} F^2(0) - F^2(\pi) \\ + \int_0^\pi \frac{1}{\sin(\Theta/2)}\frac{\mathrm{d}}{\mathrm{d}\Theta}F^2(\Theta)\mathrm{d}\Theta \end{array}\right]\right\}, \tag{27}$$

and the Waterman-Truell equation [26]

$$\left(\frac{k_2}{k_0}\right)^2 = 1 + \sum_j \left\{\frac{4\pi N_j(d_j)F_j(0)}{k_0^2} + \frac{4\pi^2 N_j^2(d_j)}{k_0^4}[F^2(0) - F^2(\pi)]\right\}, \tag{28}$$

were employed to reproduce the acoustic properties at finite concentrations where $N_j(d_j)$ is the number concentration of particle with the diameter d_j for the jth particle, and $F(\Theta)$ is the single particle scattering function at the angle Θ. $F(\Theta)$ is given by,

$$F(\Theta) = \frac{1}{\mathrm{i}k_0}\sum_{n=0}^{\infty}(2n+1)A_n P_n(\cos\Theta) \tag{29}$$

where P_n is the Legendre polynomials of the nth order, and A_n is the scattering amplitude [6,7,12,27–30]. While the Lloyd-Berry equation is more appropriate to describe the acoustic scattering of suspensions, the Waterman-Truell equation is also employed for the ultrasonic analysis for comparison.

The partial wave amplitude A_n of the micron-sized particle in viscous fluid was derived previously and solved by the four wave equations in terms of the radial and tangential pressure and those of displacement. Hereafter, the model is abbreviated as ECAH44 [12]. While the viscous waves are considered in the theory, the thermal contribution could be negligibly small for our micron-sized particles studied here. Then, the estimated scattering amplitude is substituted into the dispersion relation, Eqs. (27) or (28) to evaluate α and c.

4. Results and discussions

Fig. 5 shows the frequency dependences of the attenuation coefficient α, phase velocity c_L, density ρ, and thickness l, obtained for the PMMA sheet measured simultaneously by Multiple-Echo-Reflection Ultrasonic Spectroscopy (MERUS4 for solid plate). In order to acquire the broad spectra, the data were acquired using 5, 10, 20 and 30 MHz transducers covering different frequencies. The density was evaluated to be 1187 ± 8 (kg/m^3), which was in agreement with the independent experiment obtained by the floating test in a reference liquid calibrated by a pycnometer (1182 (kg/m^3), and was close to the value

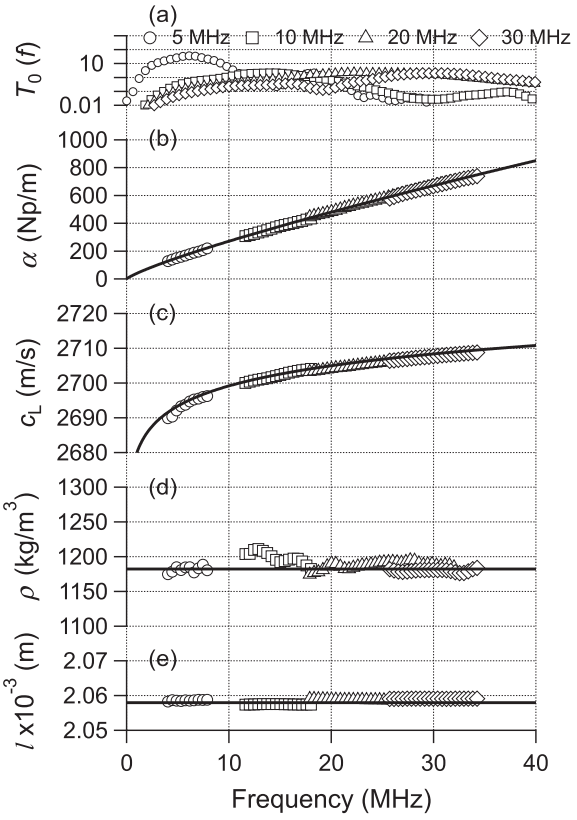

Fig. 5. (a) Transmission amplitude of ultrasound pulse as a function of frequency using 5, 10, 20 and 30 MHz transducers, and the frequency dependences of (b) α, (c) c_L, (d) ρ and (e) l of the PMMA sheet.

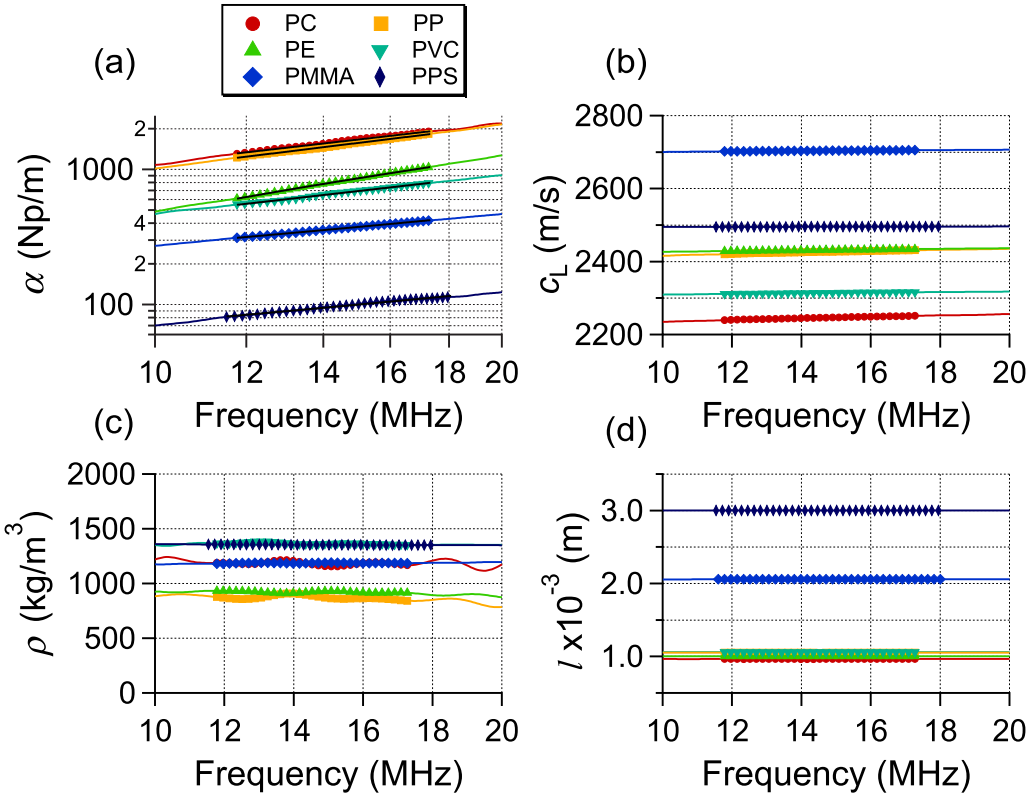

Fig. 6. Frequency dependence of (a) α, (b) c_L, (c) ρ, and (d) l of the PC, PP, PE, PVC, PMMA and PPS sheets.

reported in the literature (1187 (kg/m^3) for atactic PMMA) [31] The thickness of the PMMA sheet was evaluated by MERUS4 for solid plate, and was also in good agreement with the value measured by a thickness gauge as indicated by the solid line in Fig. 5(e). Since the thickness of the PMMA sheet was determined ultrasonically, independent measurement of the sample thickness was no longer required. Nonlinear least-squared fitting to the attenuation spectra and phase velocity respectively gave the f (Hz)-dependent values, $\alpha = 4.70 \times 10^{-4} \times f^{0.82}$ (Np m^{-1}) and $c = 2566 \times f^{0.0031}$ (m/s) at 4–34 MHz. These coefficients are subsequently used in the scattering analysis of suspension as the given physical properties of particle.

In order to demonstrate the potential of the MERUS4 technique (for solid plate), similar experiments were carried out for various plastic sheets using B10K2I. Fig. 6 shows the frequency dependences of (a) α, (b) c_L, (c) ρ, and (d) l obtained for the PC, PP, PE, PVC, PMMA and PPS plates. As shown in Fig. 6(a), the frequency dependences of the attenuation coefficient were represented by a power-law with exponent n. The evaluated exponents and the values of α / f^n were summarized in the Table 2. Similar data were also reported in the literature for PP, PE and PMMA at 1 MHz [32]. The longitudinal velocity and the density of PC, PP, PE, PVC and PPS averaged over 12 to 17 MHz were also summarized in the table. For PMMA, the data was evaluated in the wider frequency range 4 – 34 MHz as shown in Fig. 5. As shown in the table, c_Ls obtained for the various plastic sheets were close to the value reported in the literature [31].

The density of these polymers was obtained by the floating test in a refence liquid calibrated using a Gay-Lussac pycnometer. Typical transmitted waveform amplitude is, for example, 100 (mV) and the noise level is 1 (mV). Therefore, the amplitude of the multiply reflected pulse being below the noise level leads to breakdown of the present method. Providing that the thickness is 2 mm, the attenuation coefficient $\alpha = -2/(0.002*3)*\ln(1/100) = 1530$ (Np/m) suggesting almost all the plastics studied here could be measured. The densities of PVC, PMMA, PPS obtained by the MERUS4 technique (for solid plate) were in

Table 2
The density, longitudinal phase velocity, and exponent of PC, PP, PE, PVC, PMMA and PPS.

	Density ρ (kg/m^3)		Longitudinal phase velocity c_L (m/s)		n	α/f^n (s^n/m)
	MERUS4	Pycnometer	MERUS4	Reference [28]		
PC	1184	1192	2246	2220 (22 °C)	0.98	1.55×10^{-4}
PP	873	904	2427	2370 (22 °C)	1.04	5.41×10^{-5}
PE	923	953	2432	2370 (25 °C)	1.39	9.10×10^{-8}
PVC	1368	1368	2314	2330 (22 °C)	0.97	7.58×10^{-5}
PMMA	1187	1182	2704	2720 (24 °C)	0.82	4.70×10^{-4}
PPS	1354	1359	2496	N.A.	0.77	2.99×10^{-4}

good agreement with the values obtained by pycnometer. On the other hand, those of PC, PP, and PE exhibited some deviation. This is probably due to the large attenuation of the samples and the resultant error associated with the small signals.

The MERUS4 technique (for solid plate) simultaneously provides frequency spectra of the acoustic properties with good accuracy. The technique was now applied to study the cross-linked PDMS elastomer sheets. Fig. 7 shows (a) α, (b) c_L, (c) ρ, and (d) l of the PDMS sheets with different cross-linker concentrations. α was expressed by a power-law function of frequency with the exponent n = 1.70–1.82 irrespective of C_x. On the other hand, ρ, c_L and l were rather constant with respect to the frequency studied here.

Subsequently, the evaluated parameters extracted at the fixed frequency 14 MHz were represented in Fig. 8 in order to discuss the crosslinker concentration dependence of the acoustical parameters for the PDMS sheets. The acoustical properties of the PDMS sheets evaluated by the MERUS4 technique (for solid plate) were summarized in Table 3. α, c_L and ρ increased with C_x. Since c_L and ρ were simultaneously evaluated by MERUS4, the longitudinal modulus, $L = \rho c_L^2$, can

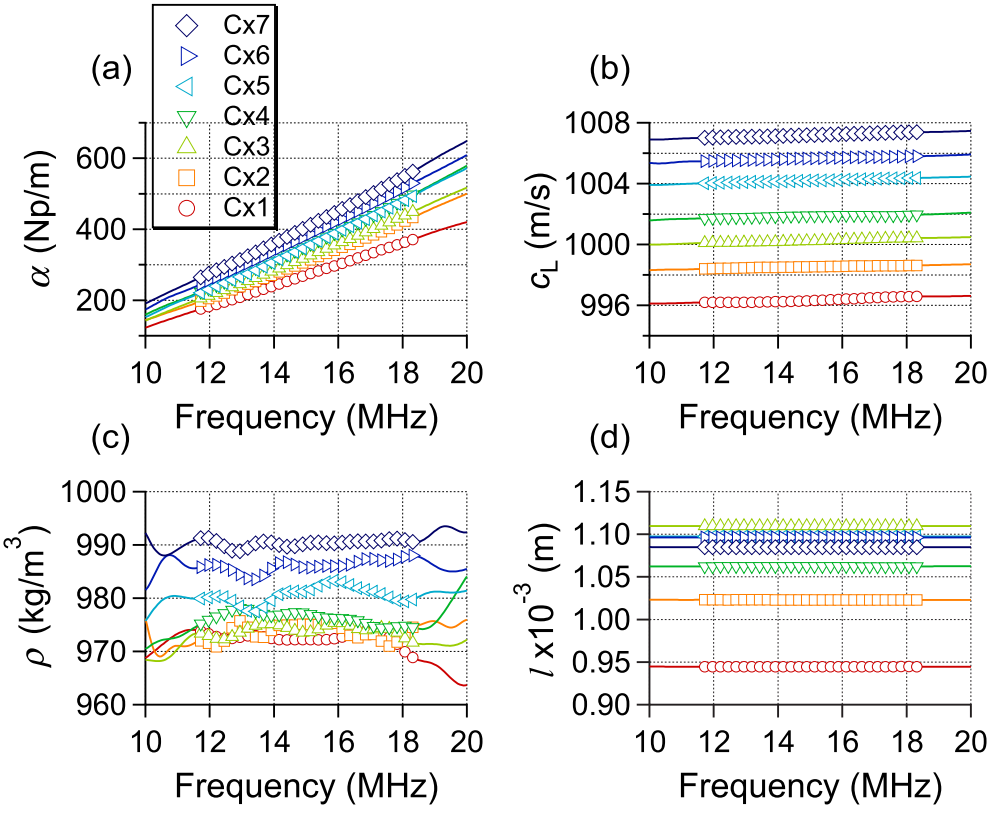

Fig. 7. Frequency dependence of (a) α, (b) c_L, (c) ρ and (d) l of the PDMS sheets with different cross-linker concentrations.

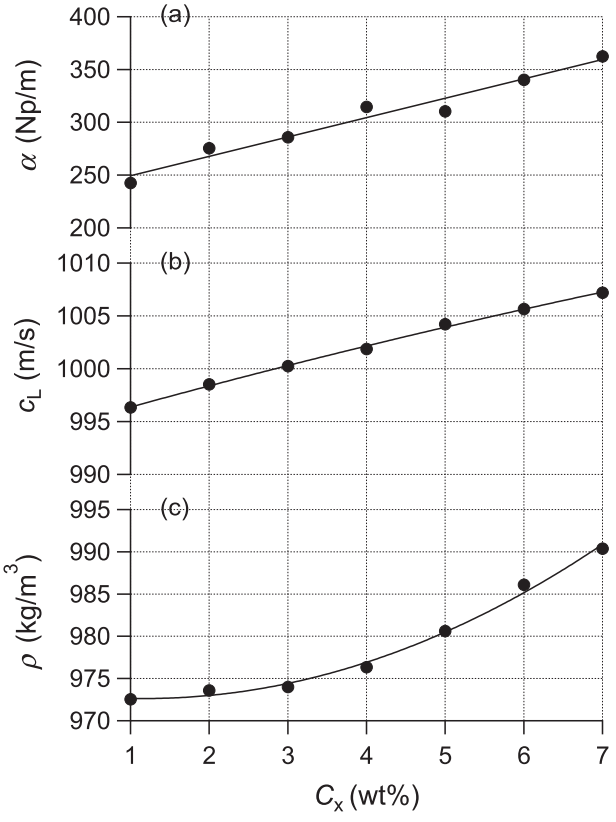

Fig. 8. The crosslinker concentration dependence of (a) α, (b) c_L, and (c) ρ obtained for the PDMS sheets.

Table 3
The density, the longitudinal velocity and the attenuation of PDMS at 14 MHz.

C_x	ρ (kg/m^3)	α (Np/m)	c_L (m/s)
1	972	243	996
2	974	276	999
3	975	286	1000
4	977	315	1002
5	980	310	1004
6	986	340	1006
7	990	362	1007

be immediately calculated.

Fig. 9(a) shows the longitudinal modulus L as a function of C_x. It was found that L linearly increased with C_x, suggesting the effective incorporation of the cross-linking point in the network. According to the classical mechanical theory, the longitudinal modulus may be described by the following equation,

$$L = K + 4/3G = \lambda + 2\mu, \tag{30}$$

where K is the bulk modulus, and G is the shear modulus G, λ and μ are the first and second lame constants. Since $\mu = G$, the bulk modulus is expressed by $K = \lambda + 2\mu/3$. In case there is no cross-links ($\mu = 0$), longitudinal modulus of bulk linear PDMS, L_0, equals to λ. Therefore, the shear modulus can be estimated by,

$$G = \mu = (L - L_0)/2, \tag{31}$$

with L_0 obtained by the following MERUS3 analysis (for liquid). The evaluated G is exhibited in Fig. 9(b). It should be noted that the longitudinal velocity and the density of linear PDMS depend on the degree of polymerization [33]. Since the PDMS elastomer sheets were synthesized by dihydroxy-polydimethylsiloxane in the presence of TEOS used as a cross-linker, the network consists of extended PDMS chains. Fig. 9(c)–(e) respectively show the dependence of α, c_L and ρ on the reaction time obtained for the linear PDMS sample without TEOS. The

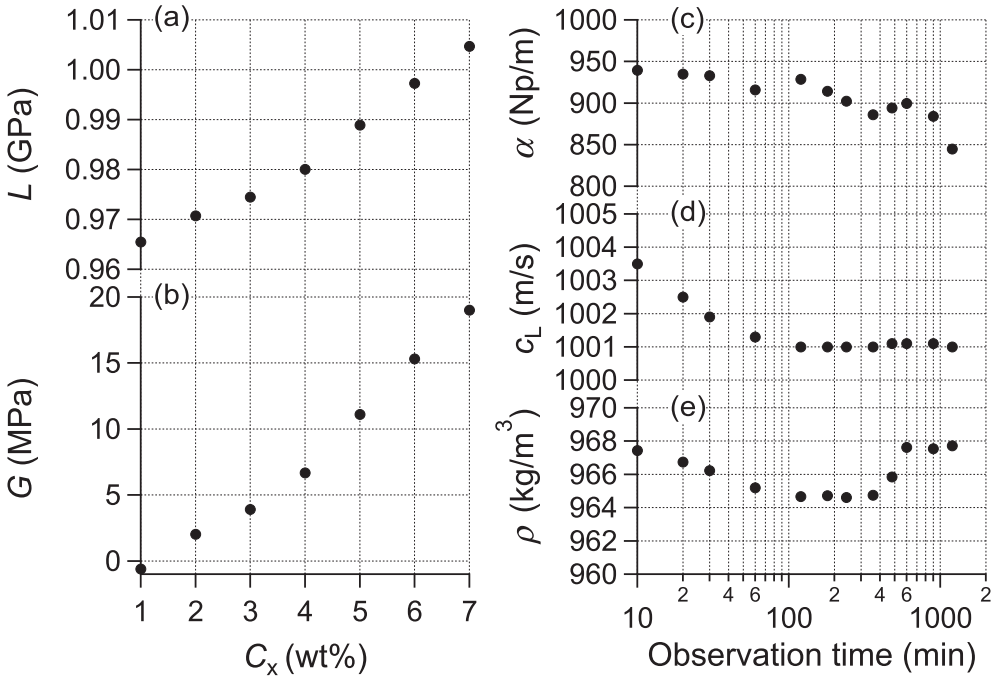

Fig. 9. The crosslinker concentration dependences of (a) L, and (b) G, of the PDMS sheets, and the polymerization time dependences of (c) α, (d) c_L and (e) ρ of the linear PDMS sample without TEOS.

data was acquired by the MERUS3 technique (for liquid) to measure α, c_L and ρ of a solution sample in a plastic vessel. The distance of the transducer (B20K2I, diameter 2 mm, 20 MHz) to sample cell was 55 mm. The values of α and c_L monotonically decreased with the observation time. In the case of the linear PDMS, the decrease in the velocity $c_L = \sqrt{L/\rho}$ was attributed to the decrease in the longitudinal modulus L (increase in the adiabatic compressibility) and/or increase in the density. As seen from Fig. 9(e), the density monotonically decreased due to reaction heat. Therefore, the decrease in c_L is probably due to slight increase in the compressibility of the material during reaction. On the other hand, the attenuation coefficient was strongly affected by the imaginary part of the longitudinal modulus. Since it is difficult to envisage that the larger molecule lead to the smaller attenuation, the decrease in the attenuation may be attributed to the frequency shift of the relaxation spectra to the lower frequency due to the chemical reaction.

Since c_L and ρ are simultaneously measured, the longitudinal modulus can be obtained in real time. In the case of the Cx1 sheet, for example, completion of the reaction requires 300–400 min. Therefore, L_0 ($=\rho {c_L}^2$) was estimated from the data based on the polymerized linear PDMS chain averaged at 300–400 min (not from precursor before reaction) with ρ = 965 (kg/m^3) and c_L = 1001 (m/s). L_0 was evaluated to be 0.967 GPa and it was subtracted from L to evaluate G with different C_xs. As shown in Fig. 9(b), G systematically increased with C_x and they were in the order of MPa, which could be a plausible value for the soft elastomer sheet in ultrasonic frequency range. The Poisson's ratios were in range 0.49 to 0.5, which were reasonable for incompressible PDMS elastomers [34–36].

Finally, acoustic scattering analysis of spherical PMMA particles dispersed in liquid with given physical constants was performed to demonstrate the validity of the scattering analysis. Fig. 10 shows the frequency spectra of (a) the sample amplitude T, (b) α ,and (c) c obtained for the PMMA particles dispersed in water with a small amount of surfactant, sodium dodecyl sulfate (SDS). The open markers show the data acquired at the different particle concentrations. The solid and dashed lines respectively indicate the theoretical curves reproduced by the ECAH44 theory with the dispersion relation of Waterman-Truell (WT) and Lloyd-Berry (LB). As shown in the figure, the theory

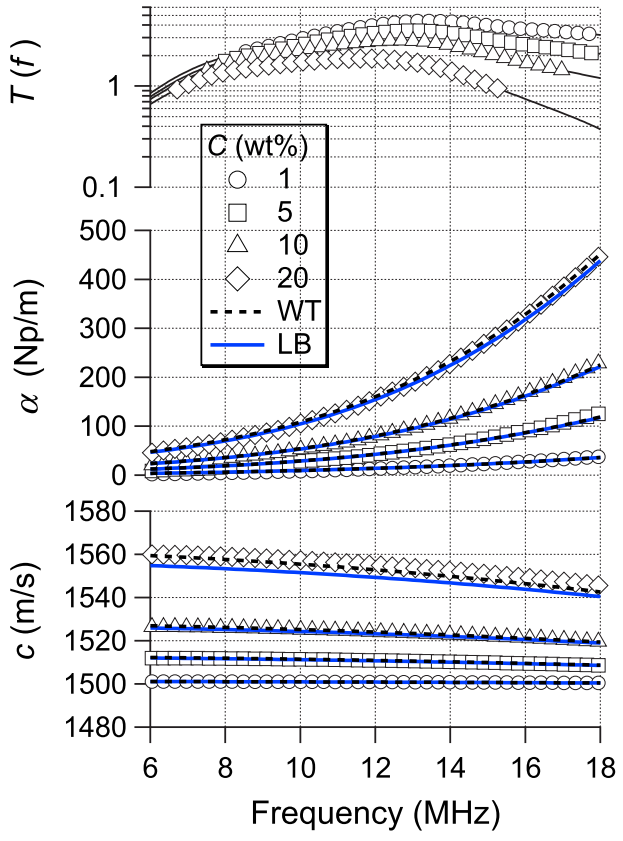

Fig. 10. The frequency dependence of (a) sample amplitude, (b) attenuation coefficient and (c) phase velocity obtained for the PMMA particle suspensions.

satisfactory reproduced the experimental results with given size distribution and density respectively evaluated by an optical microscope (size distribution) and floating test (density). As the properties of reference liquid c_{L1} = 1498.46 (m/s), $\eta_1 = 0.91225 \times 10^{-3}$ (Pa·s),

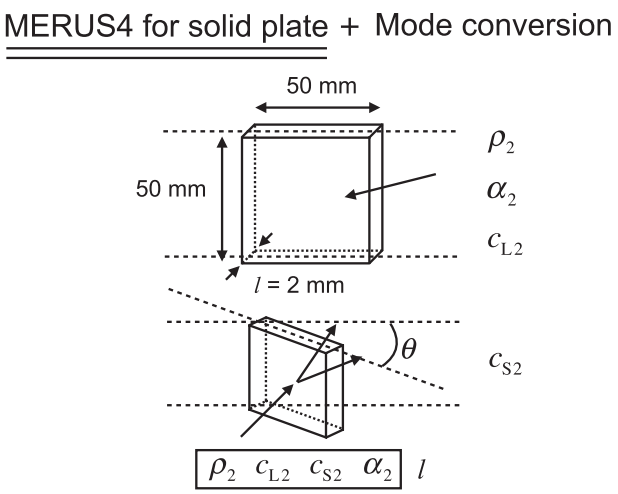

Fig. 11. The setups of (a) the MERUS4 for solid plate at normal incidence and (b) the mode-converted shear velocity measurement at oblique incidence.

$\rho_1 = 998.5$ (kg/m^3), $\alpha_1/f^{-2} = 4.88 \times 10^{-14}$ (s^2/m), are known, all the other physical constants of the sample, $c_{L2} = 2704$ (m/s), $c_{S2} = 1367$ (m/s), $\rho_2 = 1187$ (kg/m^3), $\alpha_2 = 0.00047 \times f^{-0.82}$ (m^{-1}) were determined by the MERUS4 technique (for solid plate) described above. Note that the shear velocity $c_{S2} = 1367$ (m/s) was evaluated by the mode conversion technique, namely a transmission setup at oblique incidence as schematically shown in Fig. 11. It should be also noted that the frequency spectra of the attenuation and the phase velocity obtained for the PMMA suspensions could be better reproduced by using the f (Hz)-dependent velocity of particles ($c_{L2} = 2566 \times f^{-0.0031}$ (m/s), $c_{S2} = 1264 \times f^{-0.0046}$ (m/s)) determined by MERUS4 for solid plate. By using the data evaluated by MERUS4, the frequency dependence of the attenuation coefficient and the phase velocity of the PMMA aqueous suspensions could be successfully reproduced by the acoustic scattering theories up to 20 wt%. For the PDMS sheets, direct evaluation of c_{S2} was not successful because of the extremely low shear velocity, and the difficulty of observation by the mode conversion technique.

5. Conclusions

In this study, we have demonstrated the potential of the multiple-echo reflection ultrasonic spectroscopy (MERUS4 for solid plate) to determine the frequency spectra of the ultrasonic attenuation coefficient α, longitudinal phase velocity c_L, density ρ and thickness l of the polymeric sheets. The poly(methyl methacrylate) (PMMA) particles were prepared from the PMMA solid plate by emulsification of the PMMA/acetone/toluene solution. Since determination of the fundamental properties were allowed by using the MERUS4 technique for solid plate, the acoustic spectra of the particle suspensions could be completely reproduced by the ultrasound scattering theories without any adjustable parameters. For the soft elastomer sheet of polydimethylsiloxane, the acoustical properties, α, c_L, ρ and l, are simultaneously evaluated. Although evaluation of the shear velocity c_S was only achieved for the PMMA plate (not for the PDMS sheets), simultaneous measurements of α, c_L, ρ and l, could be useful to minimize the number of adjustable parameters in the particle scattering analysis of the viscoelastic PDMS particles.

Acknowledgements

This work was supported by KAKENHI (Grant-in-Aid for Scientific Research), No. 15K05627 and 19H02776 from the Ministry of Education, Science, Sports, Culture, and Technology.

Appendix A. Supplementary material

Supplementary data to this article can be found online at https://doi.org/10.1016/j.ultras.2019.105974.

References

[1] J.-C. Bacri, J.-M. Courdille, J. Dumas, R. Rajaonarison, Ultrasonic waves : a tool for gelation process measurements, J. Phys. 41 (1980) L369–L372.
[2] P.Y. Baillif, M. Tabellout, J.R. Emery, Ultrasonic investigation of polyurethane gel forming systems, Macromolecules 32 (1999) 3432–3437.
[3] D.L. Sidebottom, Ultrasonic measurements of an epoxy-resin near its sol-gel transition, Phys. Rev. E 48 (1993) 391–399.
[4] M. Corredig, M. Alexander, D.G. Dalgleish, The application of ultrasonic spectroscopy to the study of the gelation of milk components, Food Res. Int. 37 (2004) 557–565.
[5] A.K. Hipp, G. Storti, M. Morbidelli, Particle sizing in colloidal dispersions by ultrasound. Model calibration and sensitivity analysis, Langmuir 15 (1999) 2338–2345.
[6] R.E. Challis, M.J.W. Povey, M.L. Mather, A.K. Holmes, Ultrasound techniques for characterizing colloidal dispersions, Rep. Prog. Phys. 68 (2005) 1541–1637.
[7] R.E. Challis, A.K. Holmes, J.S. Tebbutt, R.P. Cocker, Scattering of ultrasonic compression waves by particulate filler in a cured epoxy continuum, J. Acoust. Soc. Am. 103 (1998) 1413–1420.
[8] X. Ji, M. Su, J. Chen, X. Wang, X. Cai, A novel method for plastic particle sizing in suspension based on acoustic impedance spectrum, Ultrasonics 77 (2017) 224–230.
[9] V.J. Pinfield, D.M. Forrester, F. Luppé, Ultrasound propagation in concentrated suspensions: shear-mediated contributions to multiple scattering, Physics Procedia 70 (2015) 213–216.
[10] K. Kubo, T. Norisuye, T.N. Tran, D. Shibata, H. Nakanishi, Q. Tran-Cong-Miyata, Sound velocity and attenuation coefficient of hard and hollow microparticle suspensions observed by ultrasound spectroscopy, Ultrasonics 62 (2015) 186–194.
[11] T. Norisuye, Structures and dynamics of microparticles in suspension studied using ultrasound scattering techniques, Polym. Int. 66 (2017) 175–186.
[12] H. Mori, T. Norisuye, H. Nakanishi, Q. Tran-Cong-Miyata, Ultrasound attenuation and phase velocity of micrometer-sized particle suspensions with viscous and thermal losses, Ultrasonics 83 (2018) 171–178.
[13] T.N. Tran, T. Norisuye, D. Shibata, H. Nakanishi, Q. Tran-Cong-Miyata, Determination of particle size distribution and elastic properties of silica microcapsules by ultrasound spectroscopy, Jpn. J. Appl. Phys. 55 (2016) 07KC01.
[14] T. Norisuye, S. Sasa, K. Takeda, M. Kohyama, Q. Tran-Cong-Miyata, Simultaneous evaluation of ultrasound velocity, attenuation and density of polymer solutions observed by multi-echo ultrasound spectroscopy, Ultrasonics 51 (2011) 215–222.
[15] K. Takeda, T. Norisuye, Q. Tran-Cong-Miyata, Origin of the anomalous decrease in the apparent density of polymer gels observed by multi-echo reflection ultrasound spectroscopy, Ultrasonics 53 (2013) 973–978.
[16] J.P. Weight, Ultrasonic beam structures in fluid media, J. Acoust. Soc. Am. 76 (1984) 1184–1191.
[17] J.M.M. Pinkerton, A Pulse method for the measurement of ultrasonic absorption in liquids_results for water, Nature 26 (1947) 128–129.
[18] W. Marczak, Water as a standard in the measurements of speed of sound in liquids, J. Acoust. Soc. Am. 102 (1997) 2776–2779.
[19] D.K. Hsu, M.S. Hushes, Simultaneous ultrasonic velocity and sample thickness measurement and application in composites, J. Acoust. Soc. Am. 92 (1992) 669–675.
[20] K. Metwally, E. Lefevre, C. Baron, R. Zheng, M. Pithioux, P. Lasaygues, Measuring mass density and ultrasonic wave velocity: A wavelet-based method applied in ultrasonic reflection mode, Ultrasonics 65 (2016) 10–17.
[21] T. Inoue, T. Norisuye, K. Sugita, H. Nakanishi, Q. Tran-Cong-Miyata, Size distribution and elastic properties of thermo-responsive polymer gel micro-particles in suspension probed by ultrasonic spectroscopy, Ultrasonics 82 (2018) 31–38.
[22] V. Leroy, A. Strybulevych, T. Norisuye, Time-resolved ultrasonic spectroscopy for bubbles, AIChE J. 63 (2017) 4666–4672.
[23] J.G. Fikioris, P.C. Waterman, Multiple scattering of waves. II. “Hole Corrections“ in the scalar case, J. Math. Phys. (N.Y.) 5 (1964) 1413–1420.
[24] L.L. Foldy, The multiple scattering of waves. I. General theory of isotropic scattering by randomly distributed scatterers, Phys. Rev. 67 (1945) 107–119.
[25] P. Lloyd, M.V. Berry, Wave propagation through an assembly of spheres Iv. Relations between different multiple scattering theories, Proc. Phys. Soc. 91 (1967) 678–688.
[26] P.C. Waterman, R. Truell, Multiple scattering of waves, J. Math. Phys. (N.Y.) 2 (1961) 512–537.
[27] P. Epstein, R.R. Carhart, The absorption of sound in suspensions and emulsions. I. Water fog in air, J. Acoust. Soc. Am. 25 (1953) 553–565.
[28] J.R. Allegra, S.A. Hawley, Attenuation of sound in suspensions and emulsions: theory and experiments, J. Acoust. Soc. Am. 51 (1972) 1545–1564.
[29] V.C. Anderson, Sound scattering from a fluid sphere, J. Acoust. Soc. Am. 22 (1950) 426–431.
[30] J.J. Faran, Sound scattering by solid cylinders and spheres, J. Acoust. Soc. Am. 23 (1951) 405–418.
[31] N. Lagakos, J. Jarzynski, J.H. Cole, J.A. Bucaro, Frequency and temperature dependence of elastic moduli of polymers, J. Appl. Phys. 59 (1986) 4017–4031.
[32] D. Zellouf, Y. Jayet, N. Saint-Pierre, J. Tatibouët, J.C. Baboux, Ultrasonic spectroscopy in polymeric materials. Application of the Kramers-Kronig relations, J. Appl.

Phys. 80 (1996) 2728–2732.
[33] A. Weissler, Ultrasonic investigation of molecular properties of liquids. III.1 linear polymethylsiloxanes2, Amer. Chem. Soc. 71 (1949) 93–95.
[34] T. Kawamura, K. Urayama, S. Kohjiya, Multiaxial deformations of end-linked poly (dimethylsiloxane) networks. 1. Phenomenological approach to strain energy density function, Macromolecules 34 (2001) 8252–8260.
[35] B. Wang, S. Krause, Properties of dimethylsiloxane microphases in phase-separated dimethylsiloxane block copolymers, Macromolecules 20 (1987) 2201–2208.
[36] A. Müller, M.C. Wapler, U. Wallrabe, A quick and accurate method to determine the Poisson's ratio and the coefficient of thermal expansion of PDMS, Soft Matter 15 (2019) 779–784.